TURBULENT TWO-DIMENSIONAL JET FLOW AND
ITS EFFECT ON LASER BEAM DEGRADATION

By

G. D. Catalano
G. F. Cudahy
J. T. Van Kuren
H. E. Wright

I   ABSTRACT

A laser beam traversing turbulence undergoes an intensity re-
duction which is correlated with the statistical behavior at re-
fractive index perturbations. The analytical relation predicts
degradation as a function of beam diameter, path length, wave number
and wave structure function. Refractive index perturbations are
approximated via the equations of state, using temperature and velocity
perturbations. An experiment was conducted in which visible wavelength
lasers traversed a well-documented two-dimensional jet. Temperature
perturbations vary from 0.25 to 1.80 $^{\circ}$K and velocity fluctuations range
from 9.2 to 30.8 m/sec. Measured central spot intensities are as low
as 18% of the undisturbed beam, depending on jet Mach number, beam
position relative to the jet exit and wavelength. The average difference
between theory and experiment is two percent in terms of far field in-
tensity.

To supplement the flow field information, a laser Doppler veloci-
meter is developed to measure both mean and fluctuating velocities.
A photon correlator is used as a signal processor.

II   INTRODUCTION

The effect that the turbulent flow field of a high subsonic Mach
number two-dimensional jet shear layer produces on a coherent light beam
is not precisely known. The refractive index perturbations cause a
decrease in the central spot intensity of the beam in the far field
because the total energy is spread over a larger area than in the un-
perturbed case. Furthermore, the long-time average at the mean location
of the central spot is decreased by beam wandering. Numerous theoretical

and experimental efforts have been presented concerning the propagation of laser beams through natural atmospheric turbulence; however, in the atmosphere the absolute intensities of the velocity, temperature and pressure perturbations are relatively low; the beam path lengths are usually long; and the turbulence scales are quite large compared to beam diameter.[1-6] Recently, lasers have been used for wind tunnel diagnostics and in certain applications involving propagation out of aircraft in which case the beams must pass through boundary layers and free shear layers.

There are numerous examples in fluid flow problems where the local turbulence intensities are very high. One of the few methods capable of obtaining meaningful measurements in a very high turbulence environment is a laser Doppler velocimeter used in conjunction with a frequency shifting device. However, it is still the notable case that very little information exists for fluid flow problems where the local turbulence intensities exceed 30%. Thus, the need exists to develop a system that can perform reliably in the high turbulence environment.

The present study was an attempt to correlate the degradation of the far field central spot intensity formed by a collimated coherent light beam traversing the high intensity turbulence of a shear layer. In addition an attempt was made to measure the spreading of the energy over a larger area in the far field (termed broadening), and the motion of the beam in the far field (called wandering).

It was necessary to design an experiment that would approximate in a controlled manner the turbulent shear layer that exists over an open cavity normal to a uniform high velocity stream. A two-dimensional jet

with a well designed settling chamber and subsonic nozzle was fabricated. This set-up also provided double shear layers for added sensitivity. The uniform velocity core-flow could be varied with Mach numbers ranging from 0.4 to 0.8 to emphasize the compressible regime. To determine if wave length and beam size relative to turbulence scale were important, two laser frequencies were used and three beam sizes were tried at each frequency. The beam traversed the turbulent jet successively at 25, 50 and 75 nozzle widths downstream from the nozzle exit.

Since the first published account of the use of a laser Doppler velocimeter (LDV) appeared in 1964, much effort has been devoted to the LDV's development. A nonintrusive fluid diagnostic technique such as laser velocimetry allows for greater flexibility in the type measurements that can be made in a given flow situation.

In the past, the common techniques for signal analysis and information retrieval have often required relatively high powered lasers and sophisticated electronics. In addition the two most common processing schemes (i.e. (1) counter and (2) tracker) each required the inclusion of a light scattering marker in the flow. A recent advance in data acquisition utilizing the laser Doppler velocimeter technique involves the use of a photon correlator. Photon counting techniques offer improved system sensitivity by allowing velocity measurements to be made even when there are insufficient signal photons available to define the classical scattering signal.

In order to examine the effect(s) of high turbulence levels and/or high mean velocities, the LDV setup is used to monitor the velocity field of a compressed air jet. The data obtained from the LDV is compared to hot-wire anemometer data when appropriate.

III   SUMMARY

A summary of the significant results obtained in this experiment will now be given.

This investigation correlated the degradation of the far field central spot intensity formed by a collimated coherent light beam traversing high intensity turbulence with the statistical behavior of the turbulence generated refractive index perturbations causing the degradation. Since refractive index perturbations could not be readily measured a method to approximate these perturbations, via the equation of state, using velocity and temperature perturbations was developed. The turbulence quantities measured were path length, velocity correlation function and temperature correlation function. The path length had a minimum at the 25 cm test station. The rms velocity perturbations had a maximum of 30.8 m/sec at the 25 cm test station at 0.8 Mach and on an axis minimum of 9.2 m/sec at the 75 cm test station at 0.4 Mach. The corrected temperature perturbations had a maximum of 1.89 $^{\circ}$K and minimum of 0.25 $^{\circ}$K at the above respective test stations and nozzle exit flow conditions.

The actual far field central spot intensities were measured. The 4416 $\overset{\circ}{A}$, 50 mm beam traversing the 25 cm test station when the nozzle exit velocity was 0.8 Mach had an intensity of 18 percent of the reference intensity. At the 75 cm test station, with 0.4 Mach nozzle exit velocity the 6328 $\overset{\circ}{A}$, 11.0 mm laser beam had a far field central spot intensity of 100 percent of the reference intensity.

The results of the experimentally measured central spot degraded intensities were compared with the analytically predicted, using

5

experimentally determined turbulence characteristics, central spot intensities. For the same laser beams traversing statistically identical flow fields, the greatest difference between experimentally-measured and analytically-predicted degraded, far-field, central-spot intensities was 8.2 percent. The average difference between the experimentally and analytically determined intensities for all test conditions was less than two percent. These results support the approximations used to arrive at the analytical expressions which predict the laser beam for far-field central spot intensity degradation caused by turbulent flow fields and yield confidence in the ability to accurately predict those degradations using readily measurable turbulent flow field statistical parameters.

It was found that the frequency shifting crystal oscillator was needed in order to determine both the local mean velocity and the local turbulence intensity in a highly turbulent portion of the flow. For example, the downstream decay of the mean velocity at the centerline of the jet was readily determined using the basic LDV without the frequency shifting device. Typically, the turbulence intensities at the centerline do not exceed 20% for the initial development region. Once the measuring volume was located in the mixing region, the turbulence served to damp the autocorrelation function so severely as to mask out the information needed to determine the mean and rms velocities.

Due to the sampling rate having an upper limit of 50 nanoseconds, high velocities create additional problems. Recalling that the Doppler shift is given by:

$$f_D = \frac{2U \sin (\theta/2)}{\lambda}$$

and if the largest shift detectable is less than 20 MHz then for very large velocities either the half angle between the intersecting beams

6

($\theta/2$) must be made very small or the wavelength of the laser light (λ) be increased. The first approach being much more practical than the latter. Reducing the angle however also reduces the spatial resolution, thus making the velocity field seem much larger than it really is and also smearing out the finer scale turbulent occurrences.

IV DATA DESCRIPTION

To document the reliability of the photon correlation laser Doppler velocimeter, measurements are made in the flow field of a turbulent jet exhausting into the atmosphere.

Mean velocities in the longitudinal direction are measured and similarity profiles are shown for varying downstream locations and different exit Mach numbers (Fig. 1). The profiles are compared to theoretical curves developed by Gortler and Tollmien.

The decay of the centerline mean velocity with downstream displacement is also shown (Fig. 2) for different Mach numbers, and compared to data obtained by use of a hot-wire anemometer (Fig. 3).

Finally, an exit velocity profile using the LDV is compared to a profile obtained by using a hot-wire anemometer (Fig. 4). Note the difference in the flow widths.

Turbulence Characteristics Used to Predict Laser Beam Degradation

The refractive index perturbations which have the major effect on the laser beam degradation of this investigation were caused by turbulence induced density variations in the active medium through which the laser beam propagates. These density variations were not amenable to direct measurement, thus the equation of state was used to determine turbulent density variations via other readily measurable turbulence quantities. It was determined that velocity and temperature perturbations could be

7

transformed into density and, subsequently, refractive index perturbations. Since the frequency response of the temperature measuring device was insufficient for the temperature field to be measured, a method was developed to correct the temperature measurements obtained with this device.

The measurement and recording of instantaneous turbulent flow field characteristics for the entire flow field area of interest for a given experimental configuration of investigation were not possible. Statistical characterization of the turbulent flow field was, therefore, resorted to, and the prediction of the laser beam degradation was then necessarily limited to average degradation.

The turbulence parameters used to predict the laser beam degradation were the spatial temperature correlation function, spatial velocity correlation function, and the path length of turbulence field thickness associated with each correlation function. The correlation functions actually measured were temporal correlation functions. These functions and Taylor's hypothesis were used to approximate the spatial correlation functions.

Figure 5 shows examples of velocity correlation functions as they appeared on the display element of the correlator and the spectrum display. The frequency response of the constant temperature anemometer was sufficient to measure the highest frequency component of the turbulent velocity field.

Figure 6 shows examples of temperature correlation functions. Two similar functions with different correlator display time bases are shown in Fig 7(a). As discussed earlier, the frequency response of the constant current anemometer system used to measure the temperature perturbations of the turbulent field of this study was insufficient for many of

8

the flow conditions experienced.

Table I lists the rms velocity perturbations, rms measured temperature perturbations, temperature correction factors, corrected rms temperature perturbations, thickness of turbulence field each of these measurements represents, and mean velocity of the flow field for each of these measurements. The Mach number and downstream test station of each set of parameters is also given.

Predicted Versus Measured Unperturbed Laser Beam Far Field Spot Profiles

In order to compare the unperturbed beam intensity profile actually detected with that which would be analytically predicted, Eq. 1 was numerically integrated with T_τ set equal to unity. This yielded the far field spot in the focal plane of the far field forming lens. Figures 7a, b, c, d, e and f show the photographs of the test beam spots as projected on the opal glass measured by the TV camera and portrayed on the oscilloscope. Figures 8 a and b show the analytically predicted beam spots. As can be seen from the photographs and plots, the predicted and measured beam spots agree quite closely for four of the six test beams.

Solution of the Laser Beam Degradation Equations

Equation 2 in combination with Eqs. 3, 4, 5, and 6 is not amenable to exact solution; thus, numerical techniques were resorted to in the endeavor to solve these equations. Simpson's Rule was used to integrate numerically the equations with "Ar" of 0.125 mm. In order to utilize conveniently the temperature and velocity correlation functions in the numerical integrations, the correlation functions were digitized values using a least squares fit subroutine.

9

The solution of Eq. 2 using Eqs. 3 and 5 for T_τ took about 50 times more computer time than the solution using Eqs. 5 and 6. The results of the numerical integration of these equations are shown in Table II. Solutions were obtained for measured input laser beam diameters and input laser beam diameters which would yield the far field spot diameters measured.

Predicted Versus Measured Turbulent Refractive Index Induced Laser Beam Degradations

Examples of the degraded far field laser beam spots as recorded on the oscilloscope are shown in Figure 9. These photographs show the long term average degraded laser beam spots as measured by the TV camera in the regular scan mode. Since these examples show little motion of the far field spot, it is apparent that any motion which contributes to the overall degradation occurs at a frequency equal to or higher than the reciprocal of the integration time of the TV camera system. This frequency of motion will be discussed further when the results of the far field measurements using the TV camera in a single line scan mode are presented. Figure 10 shows the percentages of the detected long term average central spot intensities for all laser beams, test locations and Mach numbers. Table II lists these same data along with the solution of Eq. 2 using Eqs. 3, 4, 5, and 6 for T_τ. Figure 11 shows in graphical form the detected far field spot intensities versus those predicted by the solution of Eq. 2 using Eq. 3 for T_τ with input beam diameters which would yield the far field spot diameters measured.

Laser Beam Far Field Spot Broadening and Wandering

With the TV camera in the single line scan mode, the detection system was able to detect motions with a frequency of up to 3000 Hz. Examples were made of several measurements of the beam spots with the TV camera in

10

the single line scan mode, and with several detected spots superimposed.
The area of maximum brightness closely coincided, in most cases, to the
long term average central spot intensity detected with a TV camera in
regular scan. Thus, this maximum intensity was taken as the intensity
remaining after degradation by broadening alone. The percentage of this
maximum which yields the long term average intensity was taken as the
intensity remaining after degradation by beam motion (or wandering)
alone. A laboratory schematic of the test configuration is shown in
Figure 12.

Bibliography

1. Hufnagle, R. E. and N. R. Stanley. "Modulation
   Transfer Function Associated with Image Trans-
   mission Through Turbulent Media." Journal of
   the Optical Society of America, Vol. 54, Number
   1, 1964.

2. Lutomirski, R. F., R. E. Huschke, W. C. Meecham
   and H. T. Yura. "Degradation of Laser Systems
   by Atmospheric Turbulence." The Rand Corpora-
   tion, R-1171-ARPA/RC, June 1973.

3. Lutomirski, R. F., A. R. Shapiro and H. T. Yura.
   "Experiments on Turbulence Effects in Laser
   Propagation." The Rand Corporation, WN-7063-
   ARPA, September 1970.

4. Lutomirski, R. F. and H. T. Yura. "On the
   Mutual Coherence Function of an Optical Wave in
   a Turbulent Atmosphere." The Rand Corporation,
   RM-6266-ARPA, July 1970.

5. Sutton, G. W. "Effect of Turbulent Fluctuations
   in an Optically Active Fluid Medium." AIAA
   Journal. Volume 7, Number 9, September 1969.

6. Tatarski, V. I. Wave Propagation in Turbulent
   Medium. New York: McGraw-Hill Book Company,
   1961.

12

$$\frac{I(s)}{I_o(o)} = \hat{I}(s) = \frac{\int_o^S e^{-\frac{r^2}{2R^2}} T_\tau J_o \left(\frac{2\pi rs}{F\lambda}\right) rdr}{\int_o^S e^{-r^2/2R^2} rdr} \tag{1}$$

$$\hat{I}(o) = \frac{\int_o^S e^{-r^2/2R^2} T_\tau rdr}{\int_o^S e^{-r^2/2R^2} rdr} \tag{2}$$

$$T_\tau = \exp\left[-4k^2(79 \times 10^{-6})^2 \; x \tag{3}\right.$$

$$\sum_{i=1}^{N} \left[\frac{\Delta L_i}{\bar{\Theta}_i^4} \int_o^\infty \left\{\frac{\rho_i^2 \bar{\Theta}_i^2}{2} \left[B_{ui}^2(y) - B_{ui}^2(\sqrt{r^2+y^2})\right]\right.\right.$$

$$\left.\left. + \bar{P}_i^2 \left[B_{\theta i}(y) - B_{\theta i}(\sqrt{r^2+y^2})\right]\right\} dy\right]\right]$$

$$T_\tau = \exp\left[-4k^2(79 \times 10^{-6})^2 \; x \tag{4}\right.$$

$$\sum_{i=1}^{N} \frac{\Delta L_i}{\bar{\Theta}_i^4} \int_o^\infty \left\{\frac{\rho_i^2 \bar{\Theta}_i^2}{2} \left[B_{ui}^2(\sqrt{r^2+y^2}) - B_{ui}^2(y)\right.\right.$$

$$\left. + 2B_{ui}(o) \left(B_{ui}(y) - B_{ui}(\sqrt{r^2+y^2})\right)\right]$$

$$\left.\left. + \bar{P}_i^2 \left[B_{\theta i}(y) - B_{\theta i}(\sqrt{r^2+y^2})\right]\right\} dy\right]\right]$$

$$T_\tau = \exp\left[-2.91k^2r(79 \times 10^{-6})^2 \; x \tag{5}\right.$$

$$\sum_{i=1}^{N} \left[\frac{\Delta L_i}{\bar{\Theta}_i^4} \left\{\frac{\rho_i^2}{2} \bar{\Theta}_i^2 \left[B_{ui}^2(o) - B_{ui}^2(r)\right]\right.\right.$$

$$\left.\left. + \bar{P}_i^2 \left[B_{\theta i}(o) - B_{\theta i}(r)\right]\right\}\right]\right]$$

$$T_\tau = \exp\left[-2.91k^2r(79 \times 10^{-6})^2 \; x \tag{6}\right.$$

$$\sum_{i=1}^{N} \left[\frac{\Delta L_i}{\bar{\Theta}_i^4} \left\{\frac{\rho_i^2}{2} \bar{\Theta}_i^2 \left[B_{ui}^2(o) + B_{ui}^2(r)\right.\right.\right.$$

$$\left.\left.\left. - 2B_{ui}(o) B_{ui}(r)\right] + \bar{P}_i^2 \left[B_{\theta i}(o) - B_{\theta i}(r)\right]\right\}\right]\right]$$

TABLE I

TURBULENCE PARAMETERS

TEST STATION	LOCATION y (cm)	MACH NO.	u (m/sec)	θ_s (°K)	$\sqrt{m}$	θ (°K)	ΔL (cm)	$\bar{U}$ (m/sec)
25	0	0.8	24.0	1.23	1.4	1.72	0.5	156.
25	0.5	0.8	26.4	1.31	1.4	1.83	1.0	147.
25	1.0	0.8	29.0	1.35	1.4	1.89	1.0	133.
25	1.5	0.8	30.8	1.29	1.4	1.81	1.0	114.
25	2.0	0.8	30.4	1.23	1.3	1.60	1.5	91.8
25	3.0	0.8	25.6	1.09	1.1	1.20	2.0	54.0
25	4.0	0.8	17.6	0.87	1.15	1.00	2.0	27.0
25	5.0	0.8	8.0	0.44	1.1	0.48	2.0	12.4
50	0	0.8	18.4	0.88	1.3	1.15	1.0	112.
50	1.0	0.8	19.6	0.93	1.4	1.31	2.0	107.
50	2.0	0.8	21.0	0.91	1.2	1.10	2.0	92.6
50	3.0	0.8	22.2	0.83	1.1	0.92	2.0	77.8
50	4.0	0.8	21.4	0.72	1.1	0.79	2.0	63.4
50	5.0	0.8	19.6	0.62	1.05	0.65	2.0	51.2
50	6.0	0.8	17.4	0.53	1.05	0.55	3.0	38.6
50	8.0	0.8	11.4	0.36	1.0	0.36	4.0	19.4
50	10.0	0.8	5.8	0.26	1.0	0.26	4.0	16.1
75	0	0.8	16.6	0.61	1.0	0.61	2.0	87.6
75	2.0	0.8	17.8	0.62	1.0	0.62	4.0	78.9
75	4.0	0.8	18.4	0.57	1.0	0.57	4.0	65.0
75	6.0	0.8	17.4	0.48	1.0	0.48	4.0	50.8
75	8.0	0.8	15.2	0.38	1.0	0.38	4.0	36.0
75	10.0	0.8	12.7	0.29	1.0	0.29	6.0	25.6
25	0	0.6	19.6	0.77	1.46	1.12	0.5	119.
25	0.5	0.6	21.0	0.81	1.09	1.0	1.0	112.
25	1.0	0.6	23.0	0.82	1.3	1.06	1.0	99.4
25	1.5	0.6	23.6	0.79	1.3	1.02	1.0	85.8
25	2.0	0.6	23.0	0.72	1.1	0.79	1.5	70.8
25	3.0	0.6	20.0	0.62	1.05	0.65	2.0	43.1
25	4.0	0.6	13.6	0.26	1.1	0.29	2.0	21.6
25	5.0	0.6	6.8	0.17	1.0	0.17	2.0	8.6

TABLE I

(Continued)

TEST STATION (LOCATION)	y (cm)	MACH NO.	u (m/sec)	θ_s (°K)	$\sqrt{m}$	θ (°K)	ΔL (cm)	$\bar{U}$ (m/sec)
50	0	0.6	15.4	0.54	1.05	0.56	1.0	84.4
50	1.0	0.6	16.6	0.56	1.05	0.58	2.0	81.8
50	2.0	0.6	17.6	0.56	1.0	0.56	2.0	73.2
50	3.0	0.6	17.2	0.50	1.0	0.50	2.0	61.8
50	4.0	0.6	16.4	0.44	1.05	0.46	2.0	50.1
50	5.0	0.6	15.6	0.37	1.0	0.37	2.0	39.4
50	6.0	0.6	13.7	0.31	1.0	0.31	3.0	29.2
50	8.0	0.6	9.5	0.21	1.0	0.21	5.0	16.4
75	0	0.6	12.8	0.38	1.05	0.40	2.0	61.6
75	2.0	0.6	13.4	0.39	1.0	0.39	4.0	56.4
75	4.0	0.6	13.6	0.34	1.0	0.34	4.0	47.6
75	6.0	0.6	12.8	0.28	1.0	0.28	6.0	36.4
75	10.0	0.6	9.5	0.17	1.0	0.17	10.0	17.8
25	0	0.4	13.8	0.43	1.1	0.47	0.5	81.6
25	0.5	0.4	15.2	0.43	1.2	0.51	1.0	76.6
25	1.0	0.4	15.8	0.43	1.2	0.51	1.0	68.4
25	1.5	0.4	16.2	0.41	1.2	0.49	1.0	58.2
25	2.0	0.4	15.8	0.38	1.05	0.4	1.5	48.0
25	3.0	0.4	13.0	0.31	1.05	0.33	2.0	29.6
25	4.0	0.4	9.6	0.23	1.1	0.25	2.0	16.5
25	5.0	0.4	5.0	0.17	1.0	0.17	2.0	7.3
50	0	0.4	11.0	0.29	1.1	0.32	1.0	60.8
50	1.0	0.4	11.8	0.30	1.1	0.33	2.0	57.5
50	2.0	0.4	12.4	0.30	1.0	0.30	3.0	49.6
50	4.0	0.4	11.6	0.23	1.0	0.23	4.0	35.1
50	6.0	0.4	9.4	0.23	1.0	0.23	6.0	21.4
75	0	0.4	9.2	0.25	1.0	0.25	2.0	41.1
75	2.0	0.4	9.6	0.24	1.0	0.24	4.0	39.2
75	4.0	0.4	8.8	0.23	1.1	0.25	4.0	31.8
75	6.0	0.4	8.8	0.20	1.05	0.21	6.0	26.4
75	10.0	0.4	6.3	0.16	1.0	0.16	10.0	13.6

15

TABLE II

MEASURED AND CALCULATED LASER BEAM DEGRADED INTENSITIES

λ_o (A)	LASER BEAM SIZE (mm)	MACH NO.	TEST STATION (cm)	MEASURED INTENSITY (%)	EQ. 3	CALCULATED INTENSITY (%) EQ. 4	EQ. 5	EQ. 6
6328	50.0	0.4	25	93	92.8	91.6	89.4	92.7
6328	26.8	0.4	25	94	93.6	92.9	91.1	94.2
6328	11.0	0.4	25	98	96.9	97.3	96.8	98.4
4416	50-0	0.4	25	90	85.8	83.7	79.7	85.8
4416	26.0	0.4	25	92	87.6	86.4	83.2	88.8
4416	12.3	0.4	25	97	92.9	93.7	92.4	96.0
44.6	21.0	0.4	25	92	88.8	88.2	85.5	90.7
4416	10.8	0.4	25	97	93.9	94.8	93.8	96.9
6328	50.0	0.6	25	70	72.8	69.9	63.6	74.5
6328	26.8	0.6	25	76	75.8	74.3	69.0	79.4
6328	11.0	0.6	25	86	87.7	89.7	87.6	94.0
4416	50.0	0.6	25	56	53.1	49.8	42.9	56.8
4416	26.0	0.6	25	63	58.1	56.8	50.0	64.9
4416	12.3	0.6	25	79	74.2	77.5	73.6	85.9
4416	21.0	0.6	25	63	61.6	61.6	55.4	70.2
4416	10.8	0.6	25	79	77.3	81.1	77.8	88.9
6328	50.0	0.8	25	34	40.6	38.2	31.2	45.2
6328	26.8	0.8	25	45	46.0	45.2	38.7	53.6
6328	11.0	0.8	25	67	69.1	73.5	69.9	83.2
4416	50.0	0.8	25	18	18.6	18.6	14.7	26.1
4416	26.0	0.8	25	25	24.2	25.7	21.3	35.4
4416	12.3	0.8	25	48	45.4	51.5	46.9	65.9
4416	21.0	0.8	25	25	28.4	30.8	26.2	42.0
4416	10.8	0.8	25	48	50.4	57.2	52.9	71.6
6328	50.0	0.4	50	96	95.3	95.9	94.8	97.3
6328	26.8	0.4	50	97	96.0	96.7	95.8	97.9
6328	11.0	0.4	50	98	98.4	98.9	98.6	99.5
4416	50.0	0.4	50	94	90.7	91.9	89.7	94.6
4416	26.0	0.4	50	95	92.1	93.5	91.7	95.9
4416	12.3	0.4	50	98	96.2	97.3	96.7	98.6
4416	21.0	0.4	50	95	93.o	94.5	93.0	96.6
4416	10.8	0.4	50	98	96.8	97.8	97.3	98.9
6328	50.0	0.6	50	83	83.6	85.8	82.4	91.5
6328	26.8	0.6	50	86	86.0	88.3	85.5	93.3
6328	11.0	0.6	50	95	94.1	96.0	95.0	98.3
4416	50.0	0.6	50	78	69.8	73.6	68.1	83.6

TABLE II

(Continued)

λ • (A)	LASER BEAM SIZE (mm)	MACH NO.	TEST STATION (cm)	MEASURED INTENSITY (%)	EQ. 3	CALCULATED INTENSITY (%)		
						EQ. 4	EQ. 5	EQ. 6
4416	26.0	0.6	50	81	74.2	78.4	73.8	87.2
4416	12.3	0.6	50	89	86.6	90.6	88.4	95.6
4416	21.0	0.6	50	81	77.1	81.5	77.4	89.5
4416	10.8	0.6	50	89	88.7	92.4	90.6	96.6
6328	50.0	0.8	50	60	60.7	63.4	57.8	72.8
6328	26.8	0.8	50	68	65.6	69.0	64.2	78.0
6328	11.0	0.8	50	85	83.9	87.8	86.1	93.3
4416	50.0	0.8	50	41	38.2	42.1	36.2	54.6
4416	26.0	0.8	50	51	45.2	50.2	44.8	62.9
4416	12.3	0.8	50	72	67.3	74.0	78.8	84.5
4416	21.0	0.8	50	51	50.0	55.6	50.7	68.2
4416	10.8	0.8	50	72	7.15	78.0	75.3	87.6
6328	50.0	0.4	75	97	96.9	97.5	97.0	98.2
6328	26.8	0.4	75	98	97.4	97.9	97.6	98.6
6328	11.0	0.4	75	100	99.0	99.3	99.3	99.6
4416	50.0	0.4	75	98	93.8	95.0	94.1	96.4
4416	26.0	0.4	75	97	94.9	96.0	95.3	97.2
4416	12.3	0.4	75	99	97.7	98.4	98.2	99.0
4416	2.10	0.4	75	97	95.6	96.6	96.1	97.7
4416	10.8	0.4	75	99	98.1	98.7	98.6	99.2
6328	50.0	0.6	75	91	90.6	92.7	90.8	95.9
6328	26.8	0.6	75	92	92.0	94.0	92.5	96.8
6328	11.0	0.6	75	98	96.9	98.0	97.6	99.2
4416	50.0	0.6	75	83	81.8	85.7	82.3	91.9
4416	26.0	0.6	75	87	84.8	88.5	85.7	93.7
4416	12.3	0.6	75	94	92.7	95.2	94.1	97.9
4416	21.0	0.6	75	87	86.7	90.2	87.8	94.8
4416	10.8	0.6	75	94	9319	96.2	95.3	98.3
6328	26.8	0.8	75	80	78.6	84.0	79.9	91.6
6328	50.0	0.8	75	74	75.0	80.1	75.7	89.3
6328	11.0	0.8	75	90	91.1	94.6	93.1	97.8
4416	50.0	0.8	75	57	56.6	65.3	58.1	79.8
4416	26.0	0.8	75	65	62.7	71.4	65.2	84.2
4416	12.3	0.8	75	81	80.4	87.4	84.2	94.5
4416	21.0	0.8	75	65	66.9	75.4	69.8	87.0
4416	10.8	0.8	75	81	83.3	89.7	87.1	95.7

LV
SIMILARITY PROFILES
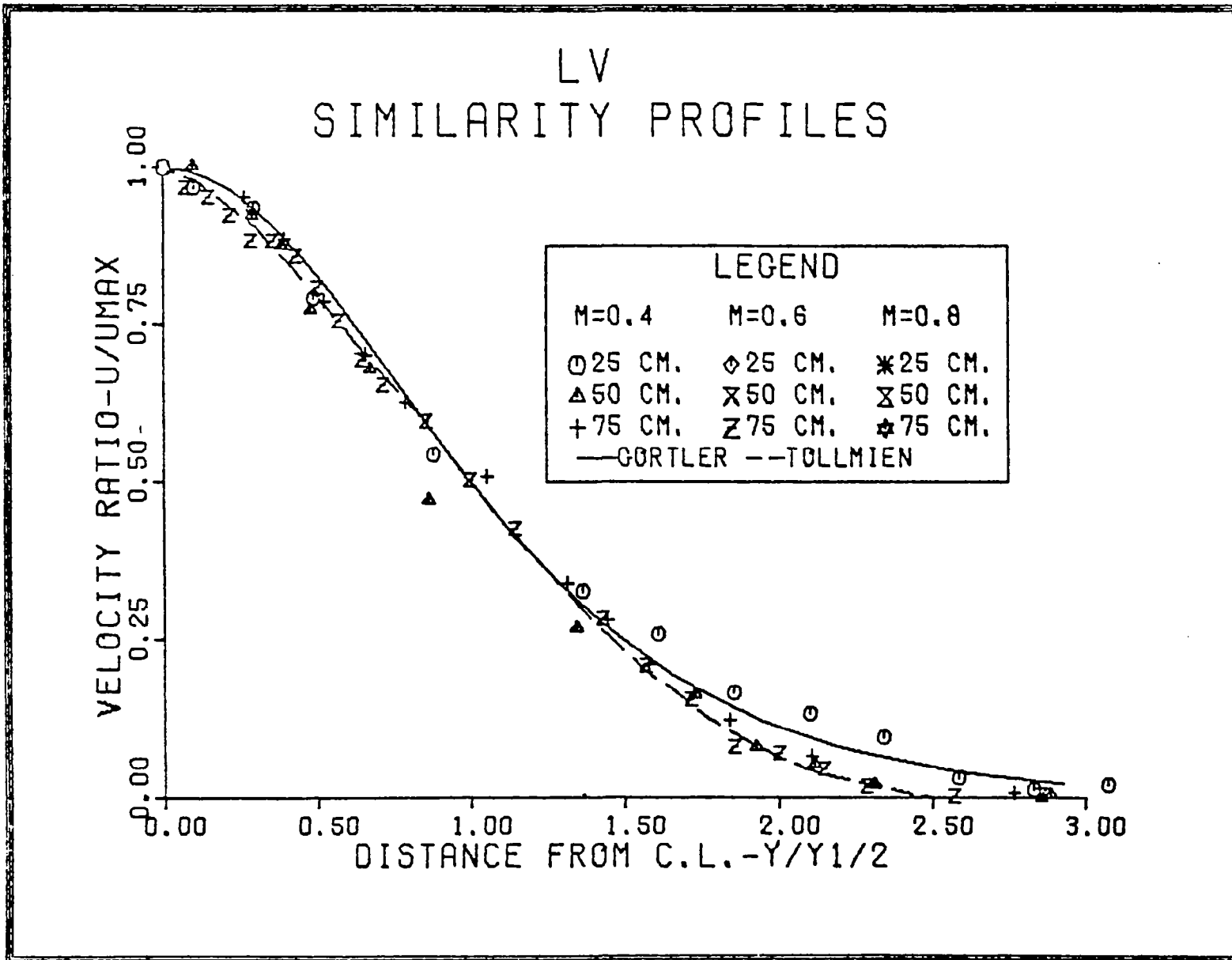
FIG. 1 LV MEAN VELOCITY SIMILARITY PROFILES.

LV
AXIAL VELOCITY PROFILE

LEGEND
- △ M=0.4
- ⦿ M=0.6
- ✿ M=0.8
- —— THEORY

VELOCITY RATIO-UCEN/UCOR

DISTANCE FROM NOZZLE-CM

FIG. 2 LV AXIAL VELOCITY PROFILE.

HOT-WIRE
AXIAL VELOCITY PROFILE

LEGEND
△ M=0.4
⊙ M=0.6
✿ M=0.8
—— THEORY
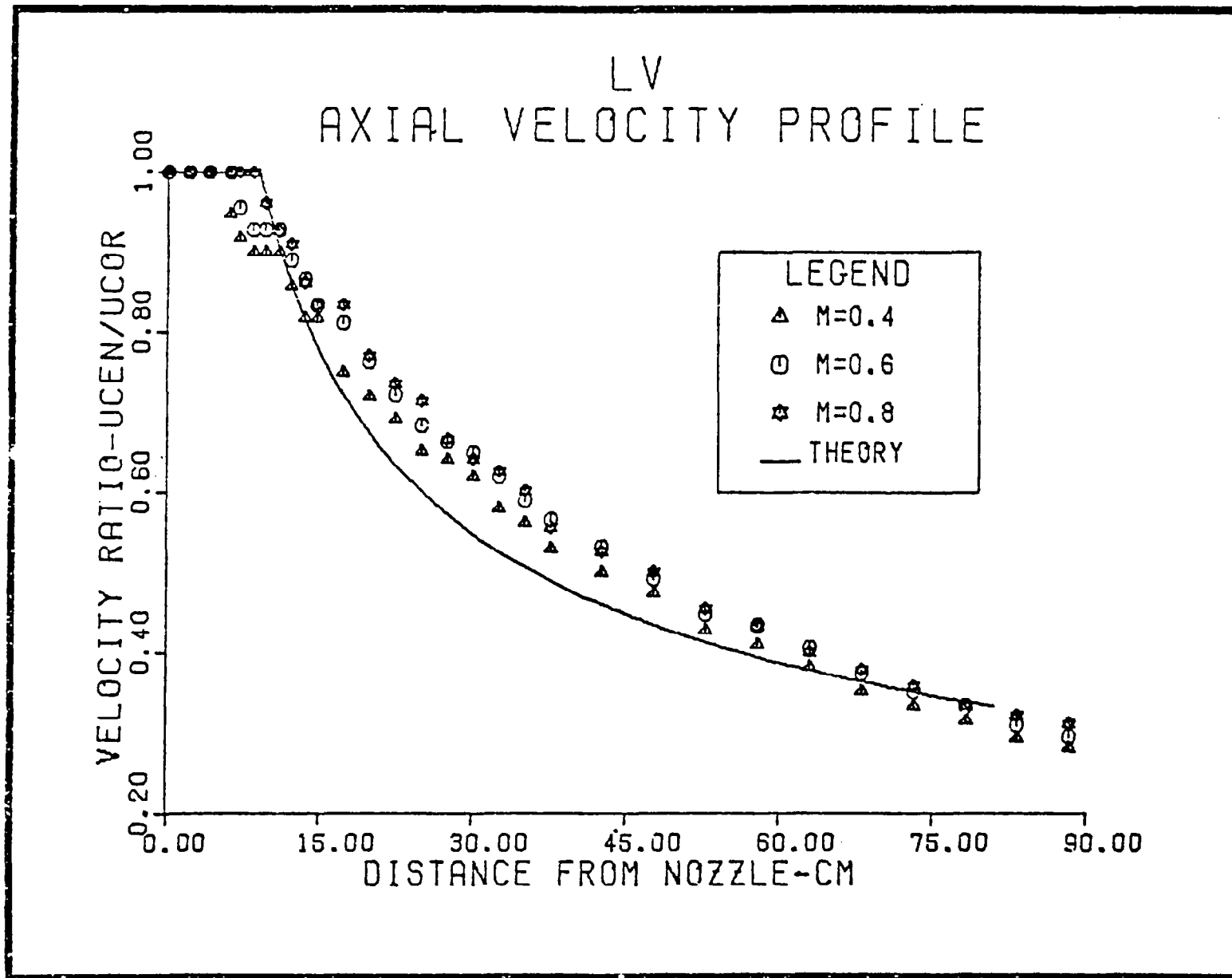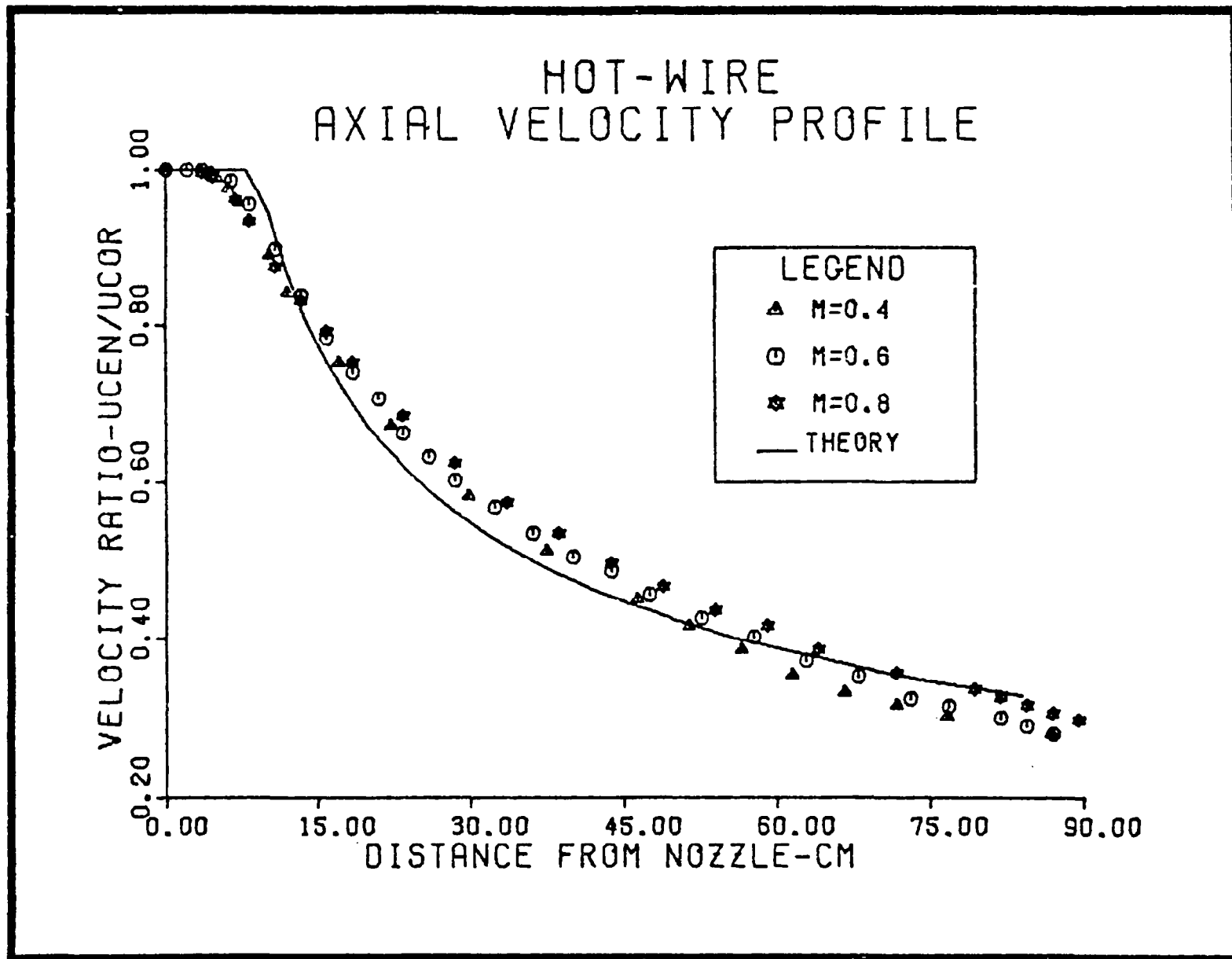
FIG. 3 HOT WIRE AXIAL VELOCITY PROFILE.

EXIT VELOCITY PROFILE
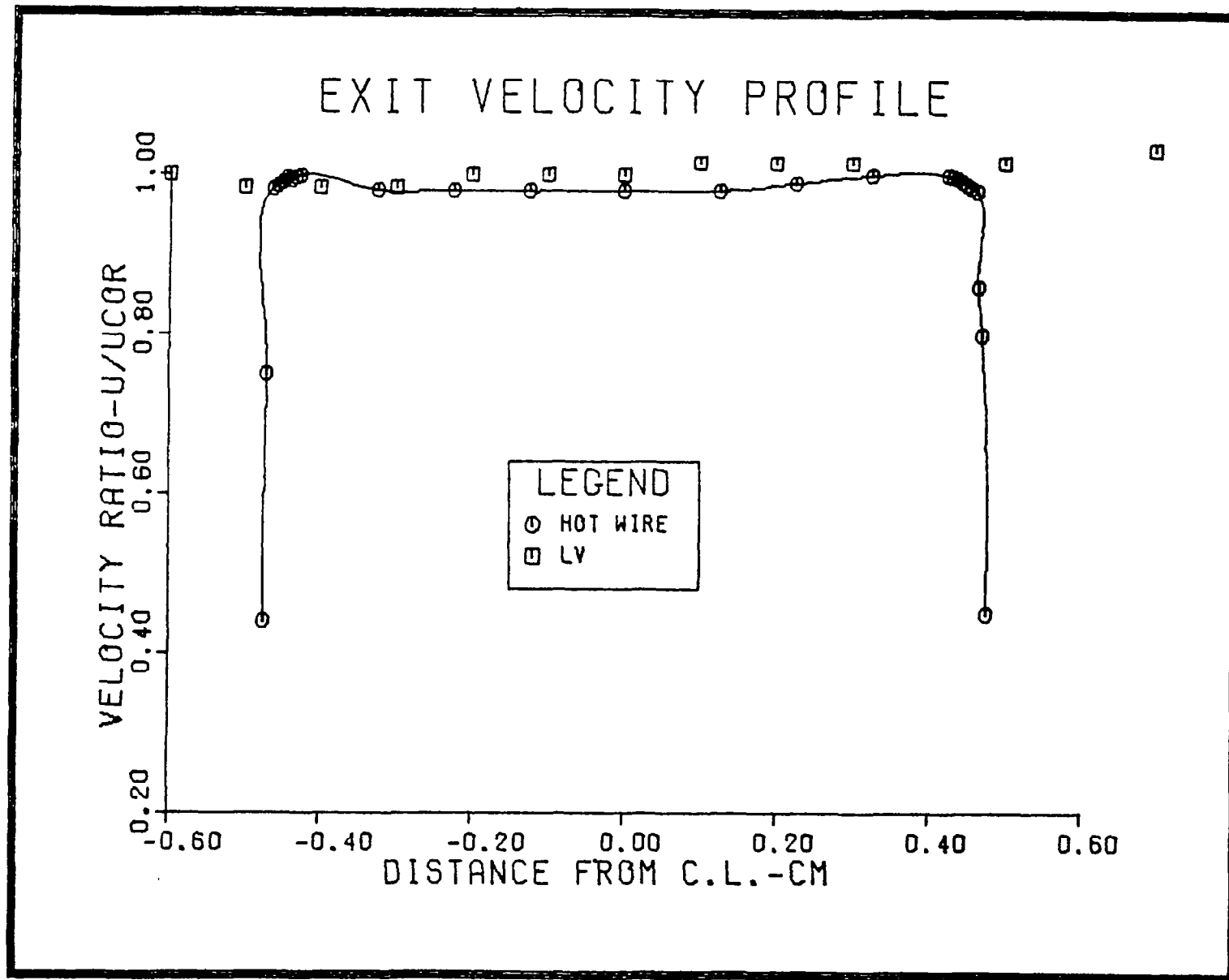
FIG. 4 HOT WIRE AND LV NOZZLE EXIT PROFILE.

Figure 5 - Velocity Correlation Functions.
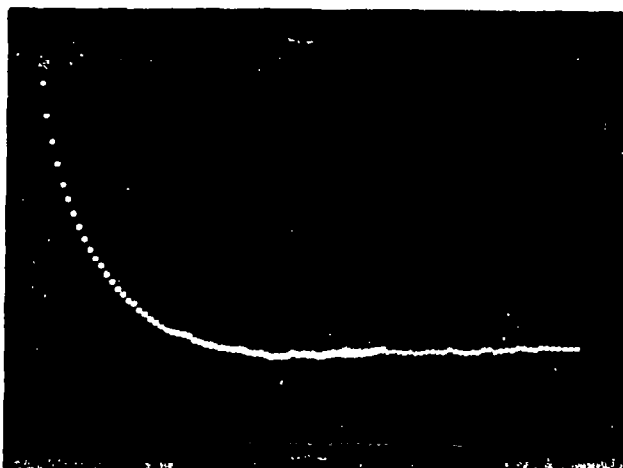
(a)   Mach 0.6   50 cm Station   Y=0 cm
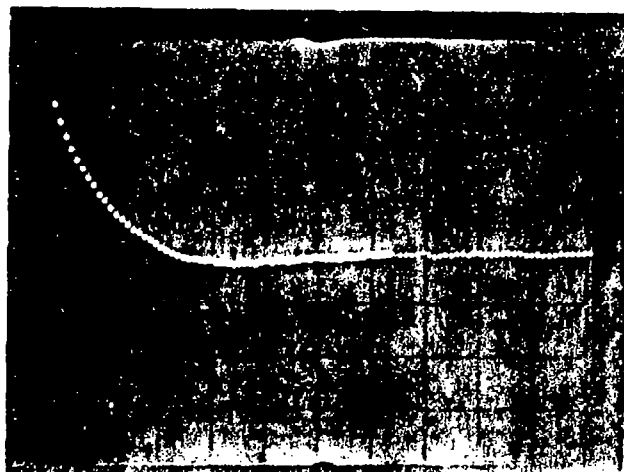
(b)   Mach 0.4   24 cm Station   Y=1.5 cm

Figure 6 - Temperature Correlation Functions.
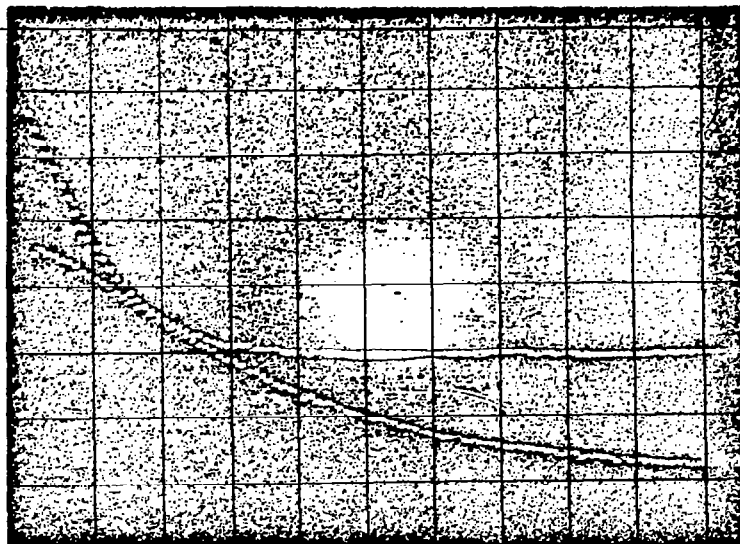
(a)   0.6 Mach, 50 cm Test Station, y = 0
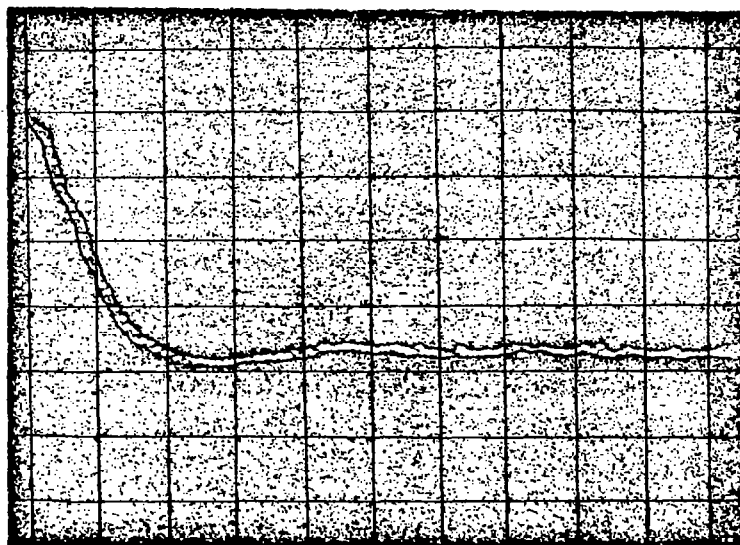
(b)   0.4 Mach, 25 cm Test Station, y = 1.5 cm

Figure 7 - Measured Beam Images.
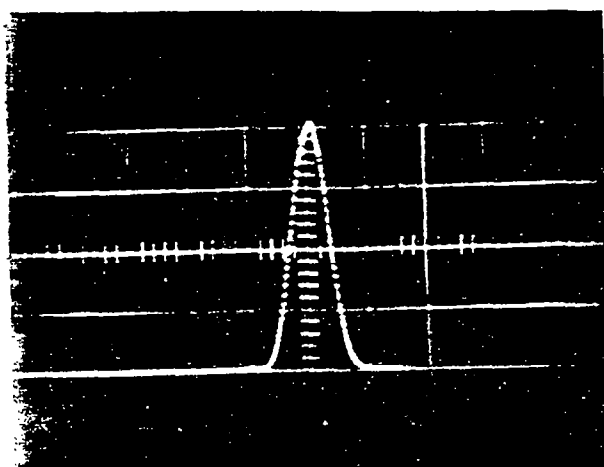
(a) 50.0 mm Beam, 6328 $\overset{o}{A}$
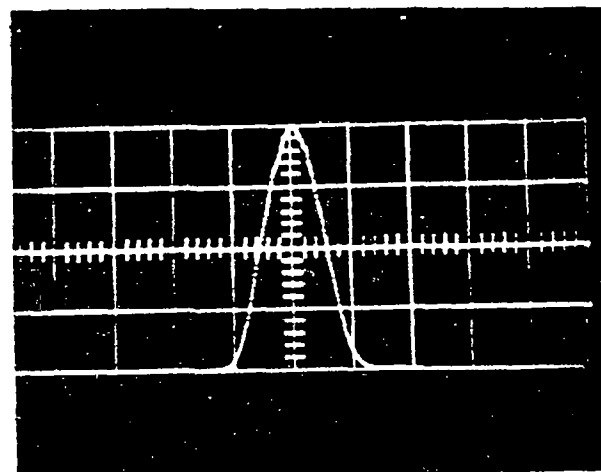
(b) 26.8 mm Beam, 6328 $\overset{o}{A}$
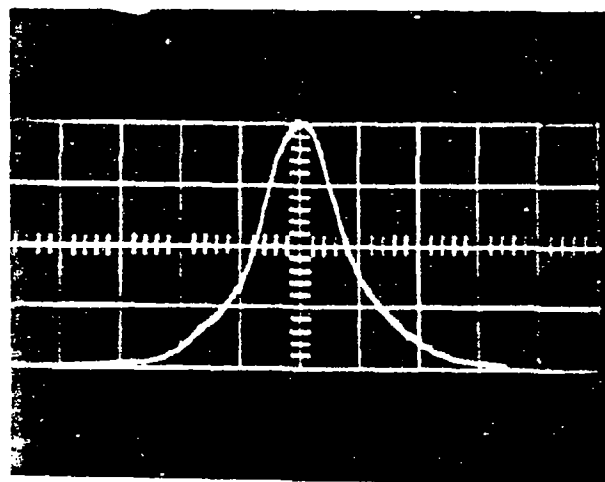
(c) 11.0 mm Beam, 6328 $\overset{o}{A}$

Figure 7 - Measured Beam Images (Cont'd).
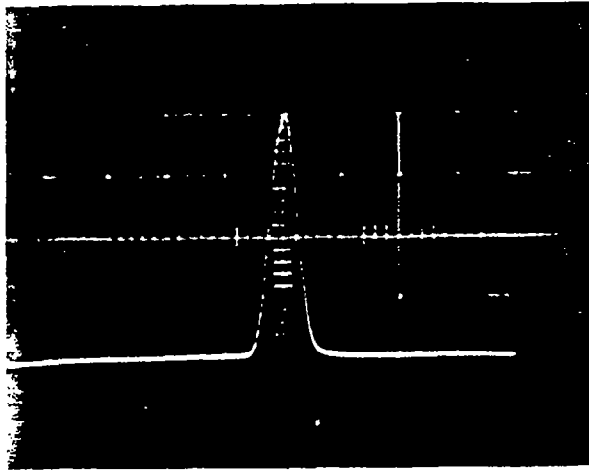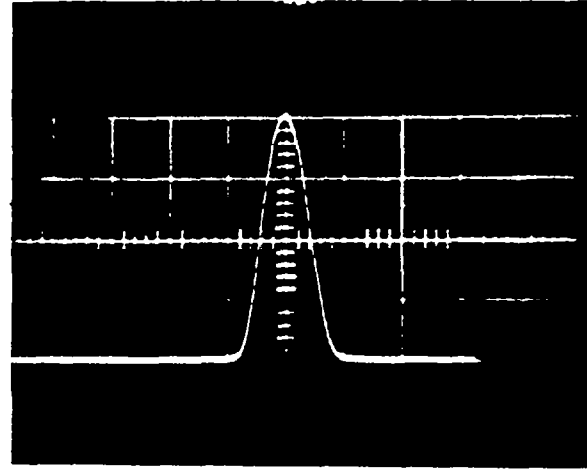
(d) 50.0 mm Beam, 4416 Å

(e) 26.0 mm Beam, 4416 Å
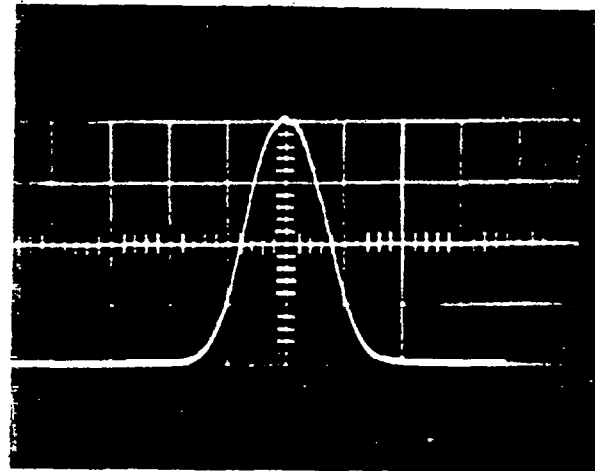
(f) 12.3 mm Beam, 4416 Å

Figure 8 - Calculated Beam Image.

(a) 6328 $\overset{O}{A}$

(b) 4416 $\overset{O}{A}$

26
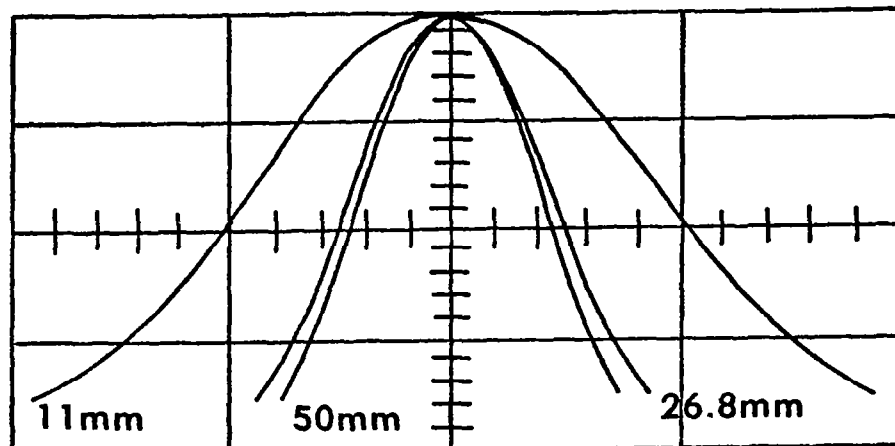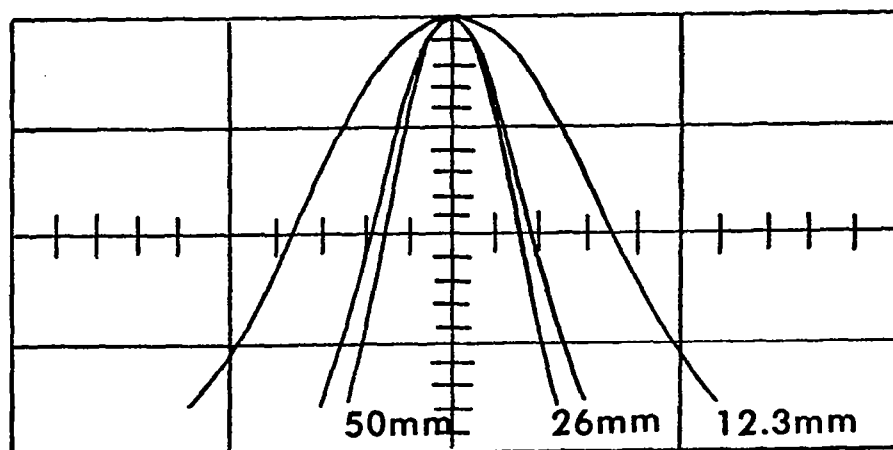
Figure 9 - Degraded Beam Images.
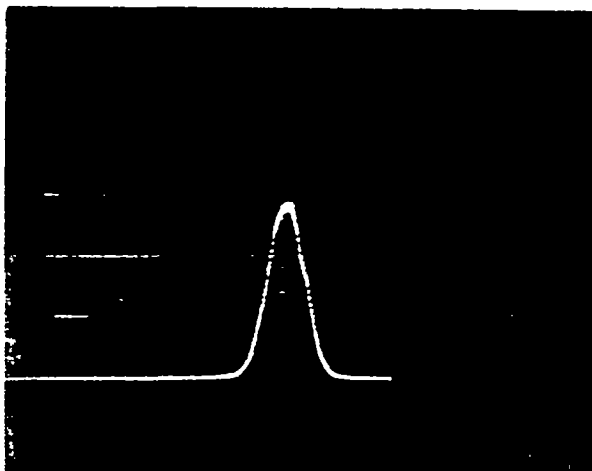
(a) 50.0 mm Beam, 6328 Å
Mach 0.6, 25 cm Station
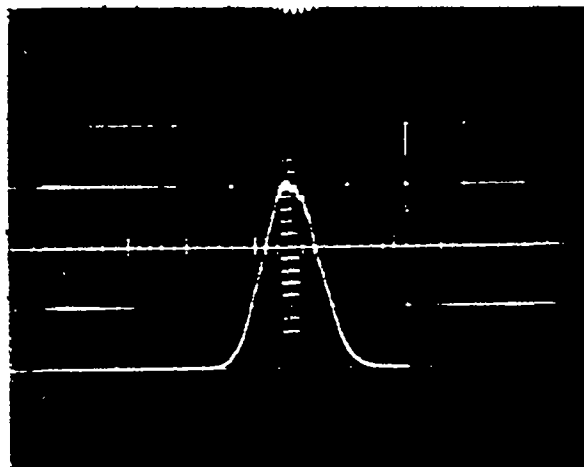
(b) 26.8 mm Beam, 6328 Å
Mach 0.6, 25 cm Station
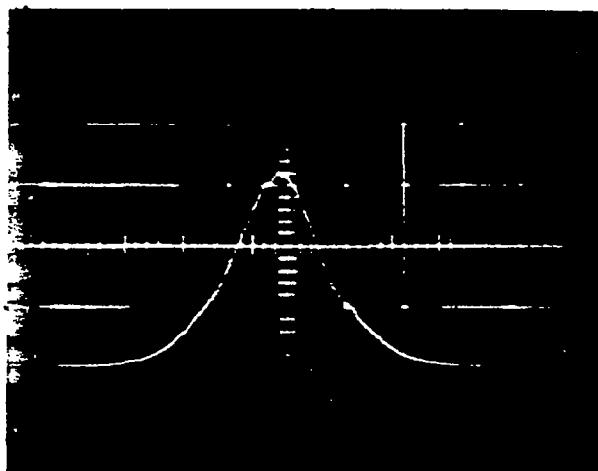
(c) 11.0 mm Beam, 6328 Å
Mach 0.8 50 cm Station

Figure 9 - Degraded Beam Images (Cont'd).
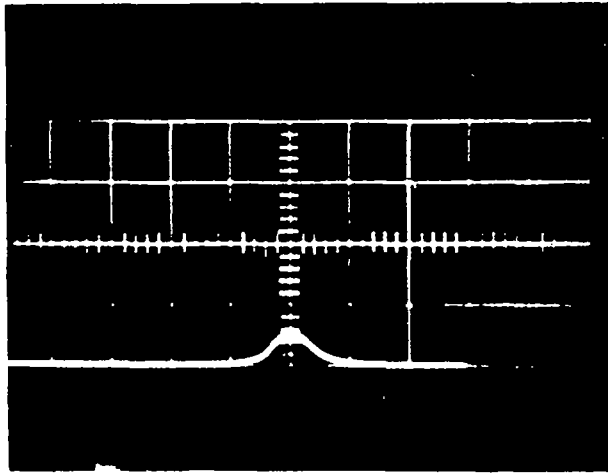
(d) 50.0 mm Beam, 4416 Å
Mach 0.8, 25 cm Station
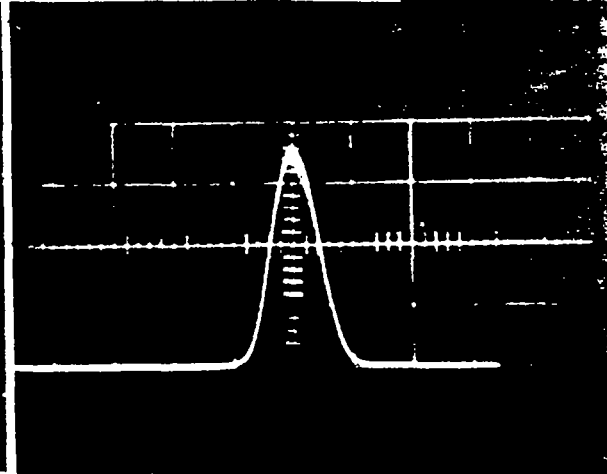
(e) 26.0 mm Beam, 4416 Å
Mach 0.6, 75 cm Station
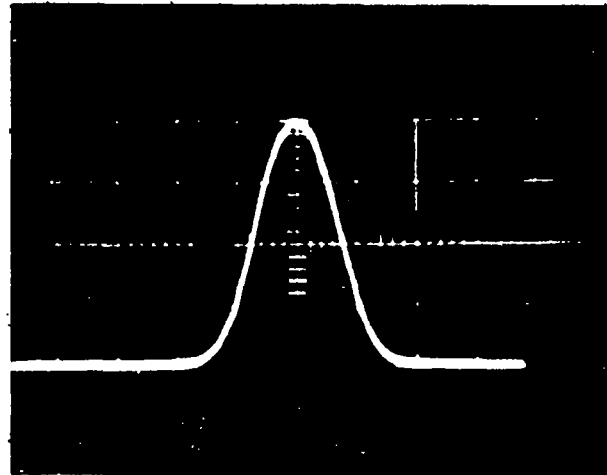
(f) 12.3 mm Beam, 4416 Å
Mach 0.4, 50 cm Station

Figure 10 - Average Degraded Intensities.
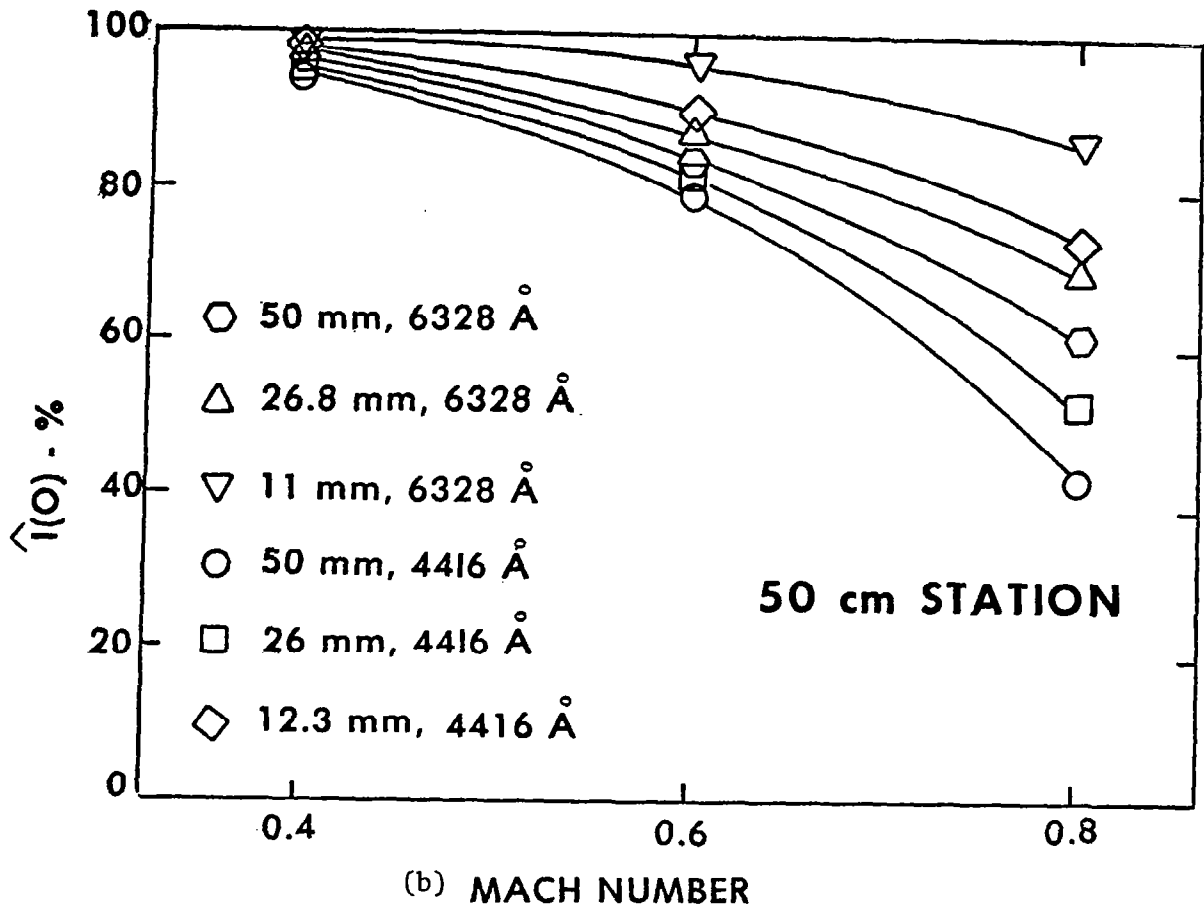

(a) **MACH NUMBER**

Figure 10 - Average Degraded Intensities.

(b) MACH NUMBER
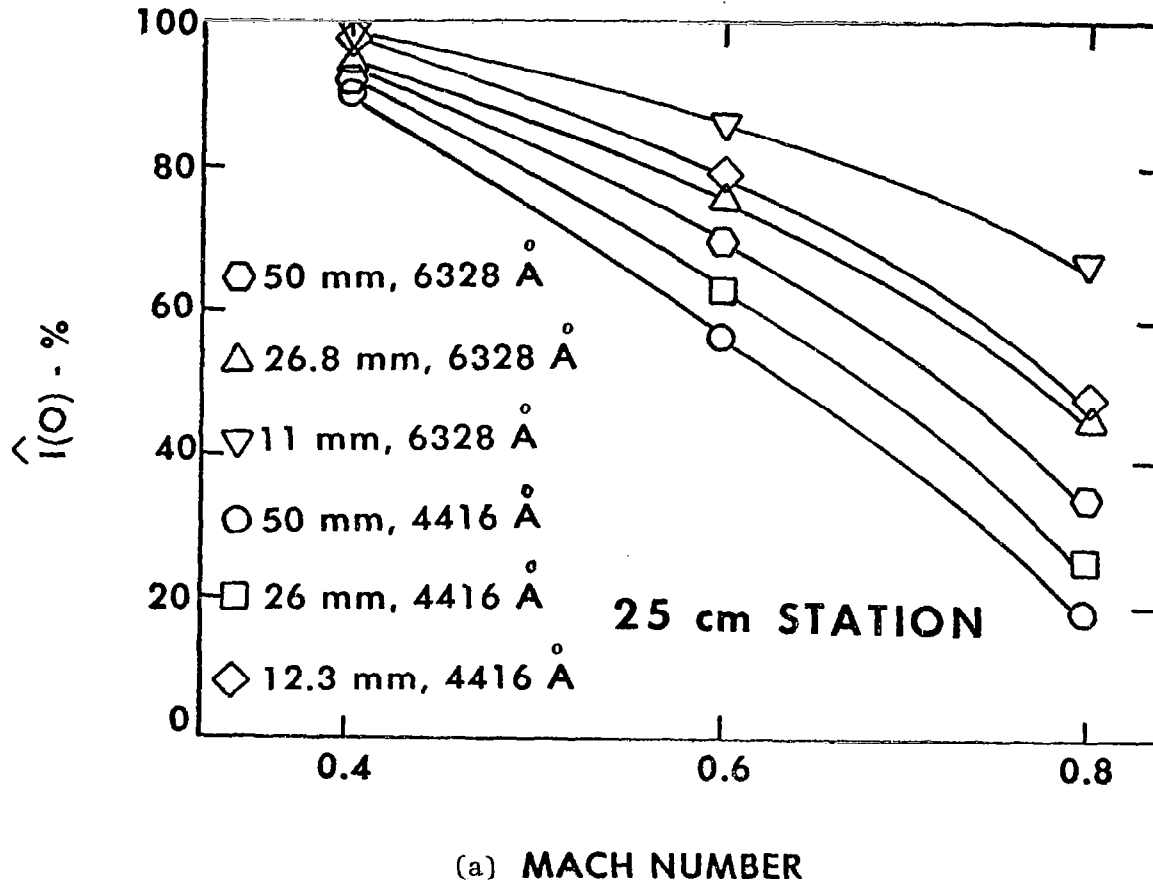
Figure 10 - Average Degraded Intensities   (Cont'd),
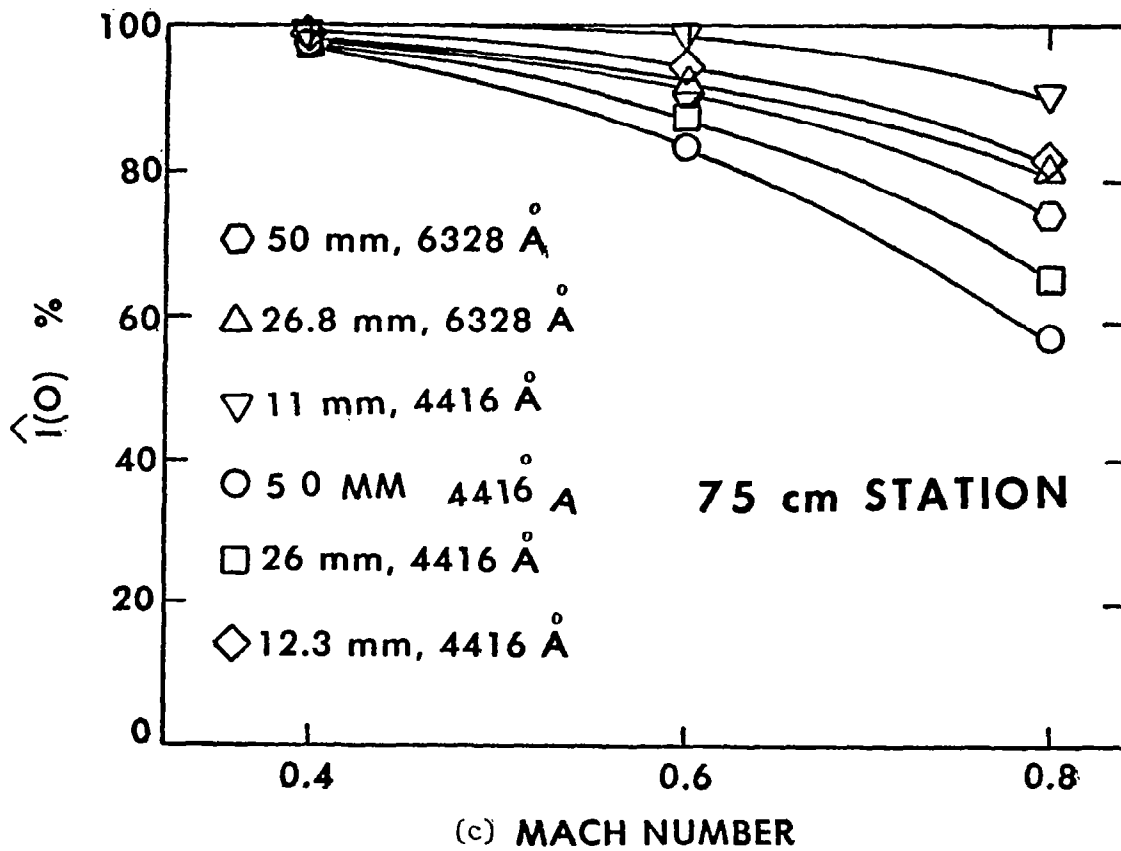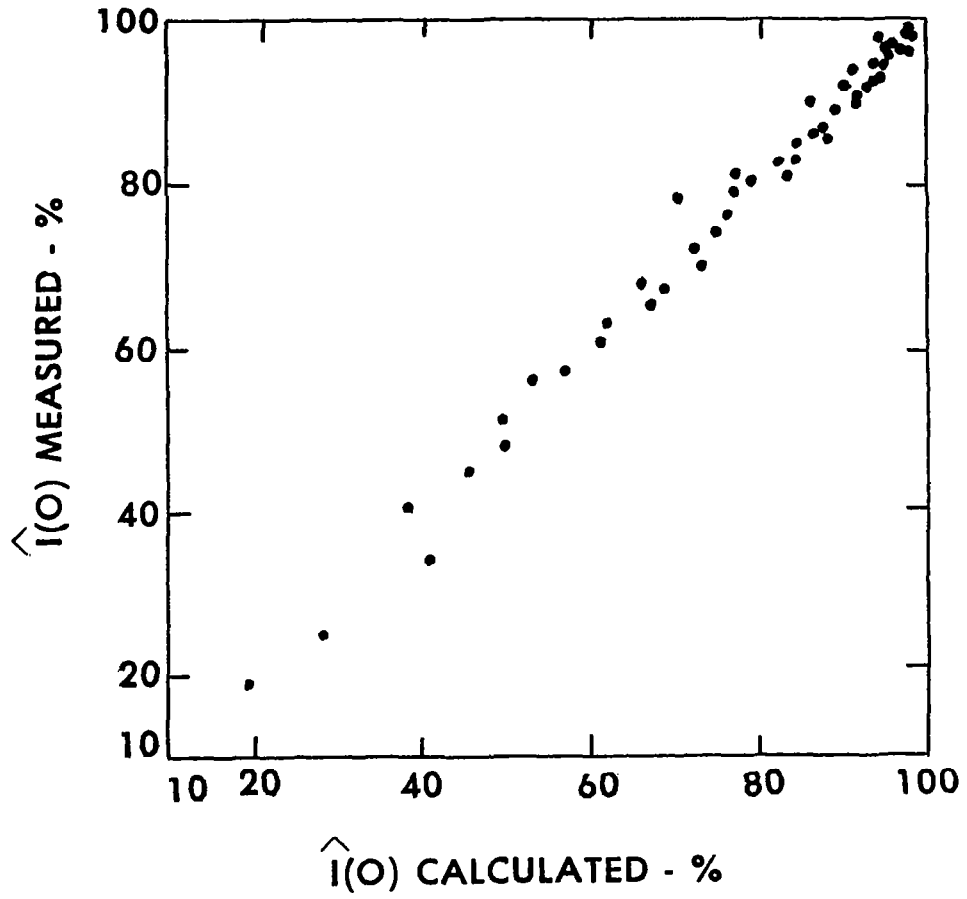

(c) MACH NUMBER

Figure 11 - Far-field Spot Intensities.

Figure 12 - Laboratory Schematic.